



Molecular hydrogen production from wastewater electrolysis cell with multi-junction $\text{BiO}_x/\text{TiO}_2$ anode and stainless steel cathode: Current and energy efficiency

Kangwoo Cho^a, Michael R. Hoffmann^{b,*}

^a Center for Water Resource Cycle Research, Korea Institute of Science and Technology, P.O. Box 131, Cheongryang, Seoul 130-650, Republic of Korea

^b Linde+Robinson Laboratories, California Institute of Technology, 1200 E. California Blvd., Pasadena, CA 91125, USA

ARTICLE INFO

Article history:

Received 21 May 2016

Received in revised form 12 August 2016

Accepted 27 September 2016

Available online 28 September 2016

Keywords:

Hydrogen

Wastewater

Electrolysis

$\text{BiO}_x/\text{TiO}_2$ anode

Stainless steel cathode

ABSTRACT

Electrochemical hydrogen evolution reaction (HER) has been recognized as a viable approach to generate a clean energy fuel. However, substantial technical breakthroughs are needed to reduce the costs for electricity and chemical reagents. In this study, we explore a specific wastewater electrolysis cell (WEC) as an alternative of decentralized H_2 production coupled with onsite water treatment. A prototypical WEC consists of a multi-junction semiconductor anode and a stainless steel cathode paired in single compartment cell. A distinct layer of $\text{BiO}_x/\text{TiO}_2$ on anode surface had relatively low crystallinity that was shown to be beneficial for higher oxide formation and O_2 evolution. The over-potential and Tafel slope of the $\text{BiO}_x/\text{TiO}_2$ anode were determined to be 0.32 V and 120 mV decade⁻¹. In a single compartment WEC with a NaCl electrolyte ($[\text{Cl}^-] \leq 50$ mM), the current density (j) ranged up to 500 A m⁻² at cell voltages less than 6 V, while the current efficiency (CE) for free chlorine (FC) evolution showed maximum value near 0.3. The CE and energy efficiency (EE) for the HER were assessed using NaCl solutions (50 mM with or without 2.5 g L⁻¹ urea) and real wastewater with variable compositions ($[\text{Cl}^-]$: 6–33 mM, [chemical oxygen demand]: 60–790 mg L⁻¹). The ohmic resistance of wastewater electrolyte rules out the usage of membrane separation, resulting in side reactions such as reduction of O_2 whose CE values monotonically decreased with an increasing j under the diffusion controlled regime. Chloride ions reduce the electron consumption during O_2 reduction, while elevated levels of FC significantly lower the CE for the HER. The combined presence of oxidizable organic compounds and Cl^- enhance the CE for the HER as long as the concentration of organics is enough to quench FC to maintain a pseudo steady-state concentration. The highest CE (0.8) and EE (0.23) for HER were observed during electrolysis of real wastewater at j values exceeding 200 A m⁻². However, a dependency of value of EE on the applied cell voltage needs to be addressed further.

© 2016 Published by Elsevier B.V.

1. Introduction

In 2014, more than 100 billion US dollars of worldwide market size was estimated for production of molecular hydrogen (H_2) as a clean and high-density energy carrier as well as chemical reagent for ammonia production and refining of petroleum and metals [1]. The major (~96%) production pathway for H_2 depends on fossil fuel transformation [2] such as the steam reformation of methane due to its cost-effectiveness. However, the carbon footprint for steam reformation to produce hydrogen has significant environmental consequences. Water splitting based on electrochemistry has been

recognized as a viable alternative way of producing H_2 from central or distributed facilities [2,3]. The concept of electrolytic H_2 production has been commercialized employing strong electrolytes in terms of alkaline [1] and PEM (polymer electrolyte membranes) electrolysis units [4]. In addition, solid oxide electrolytes [5] have been also investigated in order to improve the energy conversion efficiency. Integration of electrochemical water-splitting with renewable energy sources such as solar and wind power would serve to lower greenhouse gas emissions [3], while buffering the intermittency and fluctuations of renewable energy sources [6]. The US department of energy [7] established a target cost for the electrolytic production of H_2 to \$2.3/kg- H_2 by 2020.

A well-designed wastewater electrolysis cell (WEC) has the potential to reduce the energy requirement for electrolytic water reduction to yield H_2 via the simultaneous oxidation of the organic

* Corresponding author.

E-mail addresses: kwcho@kist.re.kr (K. Cho), mrh@caltech.edu (M.R. Hoffmann).

carbon inherently present in wastewater [8,9]. Domestic or industrial wastewater could serve as a limitless electrolyte of sufficient ionic strength and conductivity for cathodic H_2 evolution at reasonable rates and efficiencies. Chloride ions present in wastewater are readily oxidized to free chlorine (FC) species. Free reactive chlorine contributes significantly to the oxidation of organic and inorganic components in wastewater and, perhaps more importantly, to the disinfection of the treated wastewater [9,10]. The WEC might be an extended application of commercialized chloralkali processes for industrial production of chlorine from concentrated NaCl electrolytes.

The net energy savings achieved by coupling waste oxidation with H_2 production could be substantial. In an ideal case where the chemical oxygen demand (COD) is sole source of electrons for H_2 (i.e., no water oxidation), 500 mg L^{-1} of COD would produce 31 mol of H_2 (2.4 kWh from higher heating value) from 1 m^3 of wastewater. For this exemplified case, the average energetic cost for domestic wastewater treatment (0.6 kWh m^{-3} [11]) could be as high as 15% of the energy input for H_2 generation, assuming the energy conversion efficiency up to 60% in a WEC [12]. Furthermore, the electrochemical systems as advanced oxidation processes used for the elimination of non-biodegradable persistent organic pollutants [13] would also be advantageous. The specific H_2 generation rates obtained with well-designed WEC systems should be substantially greater than the rates of biological H_2 generation from waste organics using microbial electrolysis cells, fermentation, and photolysis [3]. Further energy savings can be obtained by coupling the electrolysis cells with photovoltaic panel arrays and battery-pack storage systems [12,14]. Well-designed and optimized WEC reactor systems are a potential part of the energy-water nexus that is needed to address global water issues and clean energy generation.

The feasibility of using WEC systems for H_2 production during wastewater treatment has been assessed for synthetic [12,14–19] and real domestic and industrial wastewaters [8,9,20–22]. Water treatment using WECs has been relatively thoroughly demonstrated for various types of aqueous-phase chemical contaminants such that the treated water is suitable for discharge or reuse. The rates of chemical oxygen demand reduction (i.e., the oxidation of chemical contaminants) is most often proportional to applied current density (energy input), while the concentrations of chloride ion and oxidizable substrates determine the Faradaic efficiency of water treatment. In contrast, the current and energy conversion efficiency for H_2 generation varied over values of 40–80% and 30–60%, respectively. Given the complexity of the wastewater matrix, there are numerous side reactions observed during electrochemical water treatment that contribute to the variation in the H_2 generation efficiencies [10,16,17].

Herein, we investigate electrolytic H_2 production during wastewater oxidation using multi-junction semiconductor anode coupled with a stainless steel cathode. The current responses and efficiencies were quantified as functions of the specific energy input conditions and redox active components in wastewater. Results of this study can be used to optimize the energy conversion efficiencies during electrochemical wastewater treatment and contribute to the development of alternative methods for decentralized H_2 production.

2. Experimental

2.1. Preparation and characterization of the multi-junction BiO_x/TiO_2 anodes

The core component of the WEC used in this study is a multi-junction anode composed of mixed-metal oxide layers; $Ir_{0.73}Ta_{0.27}O_x$, $Bi_{0.9}Sn_{0.1}O_y$, and $Bi_{0.9}Ti_{0.1}O_z$ in series. The

$Ir_{0.73}Ta_{0.27}O_x$ layer in ohmic contact with the Ti support would serve as electron carrier by redox cycle of Ir(IV)/Ir(VI) couple [8,23], while the middle layer of Bi-doped SnO_2 is used to enhance the overall conductivity of the anode [24]. The surficial BiO_x/TiO_2 functionalities are expected to provide active sites for interfacial charge transfer (e.g., hydroxyl radical formation), and minimize corrosive losses of Ir from the underlying ohmic-contact layer. In previous reports [8,9,25], we have described the general thermal decomposition sequences for obtaining the multi-junction architecture, largely in accordance with a patented procedure [26,27]. The Ti base-metal was initially pretreated *via* grinding, degreasing, and etching in order to remove surface oxides and other impurities before deposition of the semiconductors. Aqueous precursor solutions used to form the semiconducting layers were prepared as follows: 72 mM H_2IrCl_6 with 23 mM $TaCl_5$ in 4 M HCl, 225 mM $SnCl_4$ with 12.5 mM Bi_2O_3 in 0.5 M HCl, and 225 mM titanium glycolate with 25 mM bismuth citrate in 1 M NH_4OH . Each mixed metal oxides layer was sequentially deposited by brushing individual precursor solutions and followed thermal annealing at a specific repetition number and temperature; 6 times at 525 °C, twice at 425 °C, and 16 times at 450 °C. The duration of annealing for each repetition was fixed at 10 min. During the initial half-repetitions (8 times) for the $Bi_{0.9}Ti_{0.1}O_z$ layer, Bi-doped TiO_2 (4 mol.% of Bi) nanoparticles were mixed with the precursor solution. The above sequence resulted in the mass loading of each layer approximately 4.0, 3.5, and 11.5 g m^{-2} , respectively.

The morphologies and compositions of the intact anodes were analyzed using a ZEISS 1550VP field emission scanning electron microscope (SEM), and an Oxford X-Max SDD X-ray energy-dispersive spectrometer (EDS) system. The elemental compositions on surface were estimated with average of 10 arbitrary sites in a point-and-identification mode. X-ray diffraction (XRD) profiles were collected using an X'pert MD (Panalytical) diffractometer with Cu–K radiation. The electrochemical activity of the multi-junction BiO_x/TiO_2 anode was assessed using cyclic voltammetry (CV) and Tafel analysis. The anode was matched with a silver chloride reference electrode (BaSi Inc.) and a Pt counter electrode in a custom-made H-cell using a fine porous-frit separator. The three-electrode configuration was allowed to equilibrate with 1 N $NaClO_4$ (pH ~ 7) or 1 N H_2SO_4 (pH ~ 0) under open circuit conditions for 30 min in a N_2 purged atmosphere. CV profiles were recorded over applied anodic potential (E_a) from 0 to 1.8 V *versus* normal hydrogen electrode (NHE) with three repetitive scans (5 mV s^{-1}) under quiescent condition. The potentiostatic responses of current (i) were collected at 15 min/5 min of bias/resting regime from 1.4 to 2.0 V NHE of E_a at 50 mV increments. A potentiostat (SP-50, Bio-Logic) was employed for control of E_a as well as monitoring of current density (j) and cathodic potential (E_c).

2.2. WEC with multi-junction BiO_x/TiO_2 anode and stainless steel cathode

The multi-junction BiO_x/TiO_2 anode and AISI 304 stainless steel cathode (geometric area: $3 \times 2 \text{ cm}^2$) were installed in parallel (separation distance = 5 mm) within a single compartment electrolysis cell. The cylindrical bench-top WEC consisted of 60 mL of working electrolyte, 20 mL of headspace, and gas-tight stopper with gas outlet. The Vycor® glass tip of the reference electrode was located in the vicinity of the anode center for control of E_a by the potentiostat. The voltammetric behavior of the WEC was characterized in terms of potentiostatic j in well-mixed NaCl solutions as functions of E_a (from 1.5 to 3.0 V NHE) and initial $[Cl^-]$ (10, 30, and 50 mM). At the same time, the concentration of free chlorine was measured at 2 min interval to quantify the specific rate and current efficiency (CE) for FC generation. For each experimental set of 6 min duration, the quasi-steady-state j values were estimated with averages for

the latter half of the electrolysis. The stationary j data were also compared with CV profiles recorded from 1.0 to 3.0 V NHE of E_a at 20 mV s^{-1} under quiescent conditions.

2.3. Characterization of H_2 evolution from the WEC

The effects of j and E_a on the hydrogen evolution reaction (HER) were probed in the WEC using 50 mM NaClO_4 solutions as an inert electrolyte. The E_a was sequentially elevated from 1.8 to 3.4 V NHE with 0.4 V increment and 30 min interval. In order to evaluate the interference of FC with the HER, an E_a of 3 V NHE was applied to the WEC using 50 mM NaCl solutions under a 2/1/1.5 h bias/rest/bias sequence. In this case, 1 mL of a 1.2 M urea solution was injected at the beginning of the open circuit so that the electron donating substance could quench the FC accumulated during the former electrolysis. Separate electrolysis was initiated in a solution with 2.5 g L^{-1} urea and 50 mM NaCl in order to monitor the reaction network during a complete batch treatment of a model wastewater. During these experiments, the headspace gas was evacuated directly in to a quadrupole mass spectrometer (QMS, Hidden Analytical) under continuous purging of Ar gas (flow rate $\sim 10 \text{ mL min}^{-1}$) while measuring the volumetric flow rate with a mass flowmeter (Bronkhorst). Small aliquots of sample (0.2 mL) were collected periodically to follow the redox transformation of Cl- and N-containing species.

The relationship between the H_2 evolution characteristics and the wastewater composition was investigated with variable mixtures of domestic wastewater and stored urine. The wastewater collected from local municipal wastewater treatment plant (Whittier, USA) was used after settling to get supernatant with COD concentration of 180 mg L^{-1} and $[\text{Cl}^-]$ of 4 mM. Urine from an Asian male (Age: 35) was mixed with the domestic wastewater and anaerobically incubated at 35°C for 2 days. The $[\text{COD}]$ and $[\text{Cl}^-]$ of the stored urine were 790 mg L^{-1} and 19 mM, respectively. The domestic wastewater was then diluted with 50 mM NaCl at volume ratios from 4:1 to 2:1, while the stored urine was mixed with the domestic wastewater with volume ratios from 1:0 to 7:3. The molar flux of H_2 was quantified during the electrolysis (E_a at 3 V NHE) of eleven wastewater samples, whose $[\text{COD}]$ and $[\text{Cl}^-]$ ranged from 60 to 790 mg L^{-1} and from 5.9 to 33 mM, respectively. In these experimental sets without an Ar purging, the gas outlet on the sealed stopper was kept open to the atmosphere for 10 min and switched to a graduated burette. The volumes of gaseous products obtained for 30 min were determined by water displacement in the burette, while the molar fractions of H_2 in the collected gas were quantified by a gas chromatography with thermal conductivity detector (Hewlett-Packard), using a 5 V/V% H_2 standard gas for calibration.

The CE for the observed products from the WEC and energy efficiency (EE) of H_2 generation were calculated as follows [9,12]:

$$\text{CE}_r = \frac{n_r \times F \times Q_r}{i} \quad (1)$$

$$\text{EE} = \frac{\text{HHV} \times Q_H}{E_{\text{cell}} \times i} \quad (2)$$

where CE_r is the apparent current efficiency of a reaction of interest including anodic evolution of O_2 ($\text{CE}_{\text{a, OER}}$), FC ($\text{CE}_{\text{a, CIER}}$) and ClO_3^- ($\text{CE}_{\text{a, ClOER}}$) as well as cathodic evolution of H_2 ($\text{CE}_{\text{c, HER}}$), n_r is the number of electrons required for the reaction r , F is Faraday constant ($96,485.3 \text{ C mol}^{-1}$), Q_r is the observed molar generation rate of product in reaction r (mol s^{-1}), i is current (A), E_{cell} is the cell voltage ($E_a - E_c$, V), HHV is higher heating value of H_2 (78 Wh mol^{-1}), and Q_H is the molar generation rate of H_2 (mol s^{-1}).

2.4. Analyses

2.4.1. Aqueous phase

Bulk pH and conductivity were measured with a pH meter (Mettler Toledo) and a portable conductivity meter (VWR International). The ohmic resistance between anode and reference electrode (R) was measured by current interruption method [28] programmed in the potentiostat. The $[\text{COD}]$ was quantified by dichromate digestion of the samples in DRB-200 COD reactor (Hach), according to the 420 nm absorbance measured in UV-vis spectrophotometer (Agilent). The chlorine and free chlorine were measured with DPD (N,N -diethyl- p -phenylenediamine) and DPD/KI reagents (Hach), respectively, based on the absorbance at 530 nm. A low range TN reagent sets (Hach) were employed for determination of total nitrogen (TN) concentrations (absorbance at 420 nm). Anions (Cl^- , ClO_3^- , NO_2^- , NO_3^-) and cations (NH_4^+) of interest were quantified by an ion chromatography (Dionex) with anion-exchange column Ionpac AS 19 and cation-exchange column Ionpac CS 16.

2.4.2. Gas phase (QMS)

In the QMS analysis with detection m/z ratios from 1 to 300, the gas molecules were ionized and screened by 70 eV electron impact and quadrupole in a vacuum ($< 5.0 \times 10^{-6}$ Torr) generated with a turbo pump. According to the NIST/EPA/NIH Mass Spectral Library (NIST11), the ion intensity profiles of the gaseous products from the WEC with NaCl and NaClO_4 solutions were unequivocally attributed to H_2 , O_2 , and water vapor, whereas N_2 and CO_2 were also detected in the presence of urea. The m/z values of 2, 18, 28, 32, 40, and 44 were chosen as characteristic m/z for H_2 , H_2O , N_2 , O_2 , Ar, and CO_2 , respectively. The signal intensity of each gas was estimated by the ion current of characteristic m/z which was calibrated based on standard fragmentation profiles provided by the supplier. The gas composition of the headspace was calculated provided that molar fraction of each gas is proportional to the signal intensity. The molar flux was calculated by converting the observed volumetric flow rate using ideal gas law, while considering conversion factors of the major gas components (1.4 for Ar, ~ 1 for the others). Additional details are provided in an earlier report by Cho and Hoffmann [29].

3. Results and discussion

3.1. Voltammetric characteristics of the WEC with $\text{BiO}_x/\text{TiO}_2$ anode and AISI 304 cathode

3.1.1. Physicochemical and electrocatalytic properties of the multi-junction $\text{BiO}_x/\text{TiO}_2$ anode

Fig. 1(a) and (b) shows the horizontal surface morphology of the multi-junction $\text{BiO}_x/\text{TiO}_2$ anode, characterized by a porous structure with locally visible particles. Our doping scheme of mixing Bi-doped TiO_2 nanoparticle slurry into the aqueous precursor allowed the three dimensional network with firmly cemented particles. The buried nano-sized particles could increase the density of surficial active site and reduce the formation of micro-fracture during the annealing processes typically found in the thermally decomposed mixed metal oxides layers [23,25]. An electrochemically active surface area analysis according to our previous report [23] estimated the integrated charge (Q^*) in a potential window below the water splitting region to be 8.26 mC cm^{-2} . For an analogous anode prepared without mixing the nanoparticles, about 15% lower value (7.05 mC cm^{-2}) of Q^* was observed. The EDS analysis (Fig. 1(c)) indicated that the topmost surface is exclusively composed of mixed oxides of Ti and Bi, since relatively short durations of annealing (10 min per repetitive deposition) were not enough to allow thermal diffusion of the underlying components (Sn, Ir,

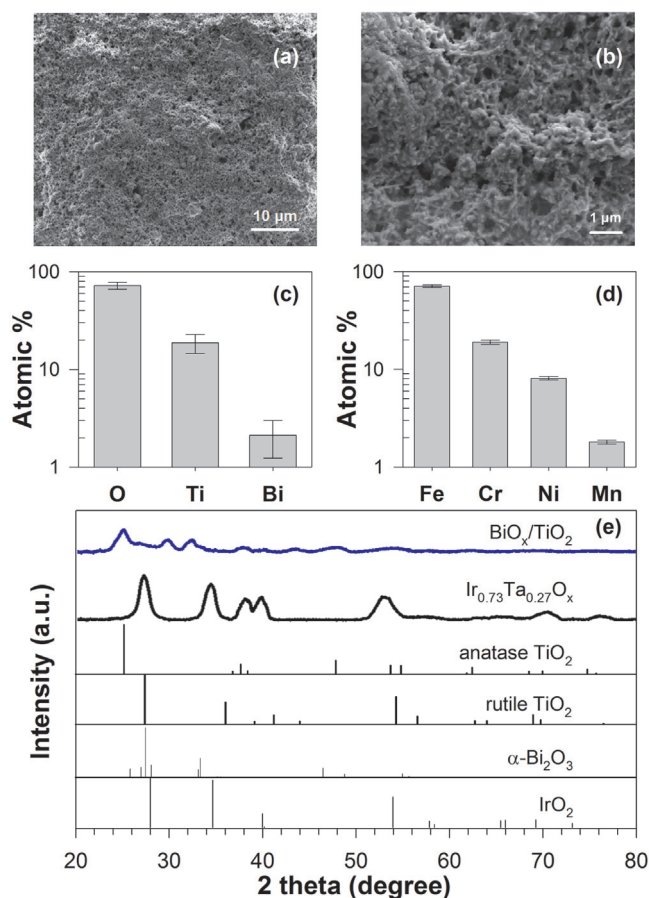


Fig. 1. SEM image on the horizontal surface of BiO_x/TiO₂ anode with magnification of 5 k (a) and 30 k (b), together with atomic fraction of major surficial elements of BiO_x/TiO₂ anode (c) and AISI 304 cathode (d) in EDX analysis. (e) Shows XRD profiles of the BiO_x/TiO₂ anode in comparison with Ir_{0.73}Ta_{0.27}O_x layer and a library for metal oxides of interests.

and Ta) towards the surface. The XRD pattern (Fig. 1(e)) of initially deposited Ir_{0.73}Ta_{0.27}O_x layer largely overlapped a standard signal of crystalline IrO₂, without interference from Ta₂O₅. Tantalum is a widely accepted secondary component in the IrO₂ based electroactive anodes for stability enhancement purposes. The Ta₂O₅ would not be miscible with IrO₂ lattice while forming amorphous secondary phase not to contribute to the XRD pattern [30]. The characteristic signals of IrO₂ disappeared after subsequent multiple junction fabrication; this is also consistent with the EDS analysis. The surficial XRD profiles of the BiO_x/TiO₂ anode showed peaks from anatase TiO₂ ($2\theta = 25^\circ$) and α -phase Bi₂O₃ ($2\theta = 33^\circ$), whose diffraction intensities were much lower than the Ir_{0.73}Ta_{0.27}O_x layer. The short annealing procedure as well as the substantial difference in effective radii of Ti⁴⁺ (61 pm) from Bi³⁺ (103 pm) [23] would bring about distortions of surface lattice structure and the comparatively low crystallinity.

The multi-junction BiO_x/TiO₂ is an active anode based on the CV and Tafel analyses. Fig. 2(a) illustrates CV profiles of the multi-junction BiO_x/TiO₂ anode in a divided cell with either 1 N H₂SO₄ or NaClO₄ solutions. The *iR*-compensated anodic potential at 1.0 A m⁻² of current density was observed to be 1.14 V at pH ~ 7 and 1.54 V at pH ~ 0, respectively, which correspond to the OER overpotential (η) of 0.32 V. A control anode without the Ir_{0.73}Ta_{0.27}O_x layer showed negligible current generation, corroborating the essential role of ohmic contact as an electron shuttle [23]. The η of Ir_{0.73}Ta_{0.27}O_x anode (without Bi_{0.9}Sn_{0.1}O_y and Bi_{0.9}Ti_{0.1}O_z layers) was estimated to be 0.35 V, slightly higher than the reported η of

IrO₂ (0.29 V [13]) due to the mixing of Ta ions. The multi-junction architecture was found to maintain or even enhance (decrease of OER η by 30 mV) the electrocatalytic activity. Kong et al. [31] reported comparable results where a heterojunction deposition of PbO₂ thin layer showed negligible effects on the OER activity of IrO₂-Ta₂O₅ anode. Considering the substantial loading (thickness) of the outer BiO_x/TiO₂ layer, the electron transfer towards the underlying Ir components is suspected to be governed by a bulk-limited conduction, rather than an electron tunneling as in the case of ultra-thin TiO₂ film [32]. The low crystallinity of the surficial BiO_x/TiO₂ layer would be beneficial in terms of an augmented concentration of coordinately unsaturated active sites for OER intermediates formation. Moreover, the OER activity of metal oxides anodes is known to be in a close relation with the enthalpy change in transition to higher oxides. Tsuji et al. [33] provided evidence that the flexibility of an amorphous structure favors the chemisorption of oxygen via structural distortion of the short-range ordered structure. In addition, the Faradaic capacitance of bismuth oxide and extrinsic oxide vacancies from Bi doping could facilitate the mobility of oxide ions. The Tafel slope values were near 120 mV decade⁻¹ at both pH conditions (Fig. 2(b)), corroborating that the rate determining step in the OER sequence is initial dissociation of water (i.e., surficial hydroxyl radical formation) and further transition to higher oxide is more facile. As a direct evidence, further annealing of the BiO_x/TiO₂ anode for longer duration (1 h) brought about overall decrease in *j* values by almost 30%, along with an increase in crystallinity (data not shown).

3.1.2. Voltammetric responses of the WEC with dilute aqueous solutions

In commercialized alkaline electrolysis systems for H₂ production, operational current densities exceeding 0.1 A cm⁻² are expected at a E_{cell} near 2 V in concentrated electrolyte solutions (e.g., 30 wt% KOH or NaOH), while even higher $j \leq 2$ A cm⁻² can be obtained when using polymer electrolyte membranes [3,4,34]. However, relatively lower electrical conductivities (σ) of wastewater may pose several limitations on a WEC system for H₂ production. The σ value of source separated urine, which is one of the most saline domestic wastes, is reported to be around 25 mS cm⁻¹ [35]; that value would decrease due to dilution in a sewer network with multiple water inputs. The cell voltage for electrochemical water treatment system is normally >3 V [9], in order to obtain current levels enough for reliable water treatment capacity. Fig. 3 illustrates the typical voltammetric response of a single compartment electrolysis cell with 10, 30, and 50 mM NaCl solutions (σ : 1.26, 3.53, and 5.50 mS cm⁻¹) under variable E_{cell} . A potentiostatic regime with an adjustable E_a required virtually an identical magnitude of E_c (half of E_{cell}) with a minimal impact of σ on the E_c value (Fig. 3b). The quasi stationary values of *j* (Fig. 3(a)) were almost superimposable on the linear sweep voltammetry, indicating negligible interference of the double layer capacitance in the estimate values. The dependency of *j* on the E_{cell} was virtually linear due to the lack of *iR* compensation [8,29]. In addition, the current responses at a given E_{cell} increased nonlinearly with the ionic concentration as expected by Kohlrausch's law in dilute aqueous solutions. As shown in Fig. 3(c), proliferations of *iR* drop become more pronounced as the E_{cell} increases and as the σ decreases. A current interruption method was used to estimate the *R* values between the anode and reference electrode; they were found to be 21.8, 6.04, and 4.17 Ω , respectively, for each solution composition. As a consequence, the decrease in current for lower chloride ion concentrations may be attributed to the combined decreases in the exchange current density and the *iR*-compensated anodic potential.

The significant *iR*-drop in the dilute aqueous solutions (wastewater) makes a usage of diaphragm or proton exchange membrane

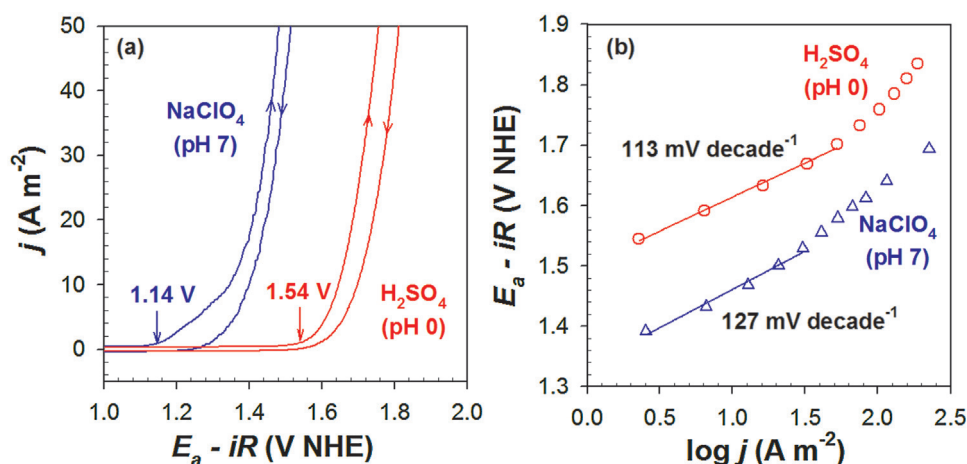


Fig. 2. Voltammetric characteristics of multi-junction BiO_x/TiO₂ anode in terms of (a) cyclic voltammetry (scan rate: 5 mV s⁻¹) and (b) Tafel plots in 1 N H₂SO₄ and NaClO₄ solutions.

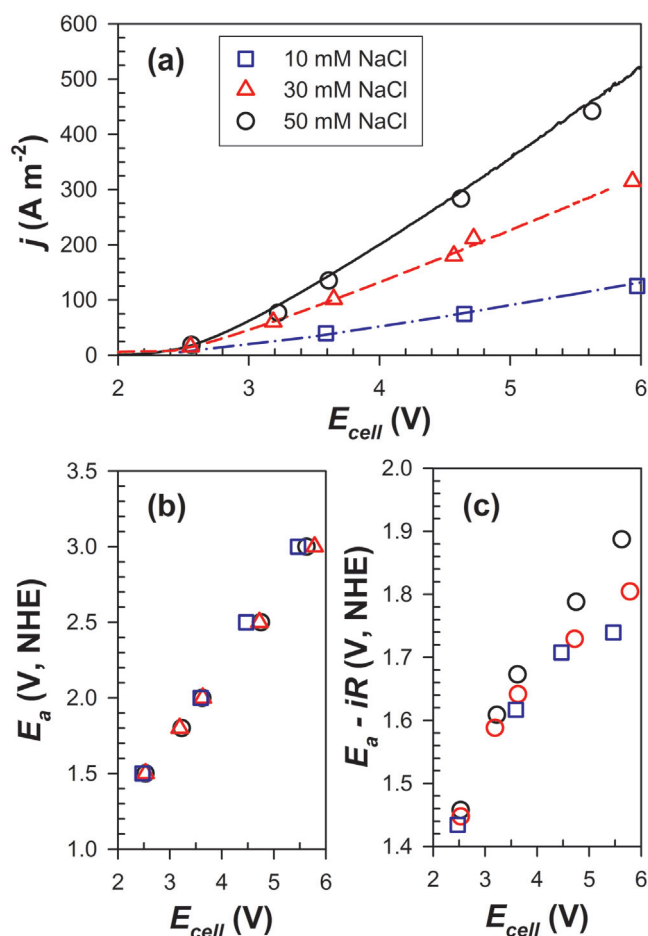


Fig. 3. Quasi-stationary voltammetric responses of a single compartment electrolysis cell with BiO_x/TiO₂ anode and AISI 304 cathode in NaCl solutions with variable concentrations. Solid lines illustrate linear sweep voltammetry from identical apparatus at scan rate of 20 mV s⁻¹.

in the WEC impractical. Therefore, several side reactions such as reduction of O₂ and FC would deteriorate the current and energy efficiency of H₂ production. Even when the ideal cathodic CE is possible, gases generated from anodic reactions (O₂, N₂, CO₂, and *et cetera*) are impurities in the membrane-less WEC, preventing a direct introduction of the gaseous products to a hydrogen fuel cell [36]. The maximum observed j value was near 500 A m⁻² at an E_{cell}

of 6 V in a 50 mM NaCl solution. The relatively high operational cell voltages in WEC systems inherently limit the energy efficiency of H₂ production, which is primarily determined by the cell voltage (*vide infra*).

3.2. Reaction networks in the single compartment WEC

3.2.1. Efficiency of water splitting in the absence of chloride ions

The HER represented by C1 in Table 1 has a well-known reaction sequence of Volmer discharge step combined with either Heyrovsky step or Tafel step. On the stainless steel (AISI 304) cathode, the active electron transfer sites are provided by Fe and Ni, especially considering their dominant surface concentrations (Fig. 1(d)) and orders of magnitude greater HER activities above those of Cr and Mn [37]. Fe is known to have a comparable H-bond strength and work function with Ni, that are principal determinants of HER activity [37,38]. In addition, evidence has been presented that binary composites of Fe and Ni show greater H₂ evolution capability than pure Fe and Ni in acidic and basic electrolytes [39–42]. Even though Fe and Ni do not approach the summit (*e.g.*, Pt, Ir) of the volcano plot for the HER, the low-cost of these earth-abundant catalysts allow Ni-doped stainless steel to be used for electrolytic H₂ evolution under alkaline [1], mildly basic [43], circum-neutral [10,12,14,16,17], and wastewater [8,9,15,20,21] pH conditions in the presence of sufficient electrolytes.

Fig. 4 shows the water splitting efficiency of a single compartment electrolysis cell with 50 mM NaClO₄ solutions under potentiostatic regime with stepwise buildup of bias. The volumetric fractions of H₂ (X_H) and O₂ (X_O) in headspace reached quasi-steady-state within 10 min for each anodic potential. The anodic CE of O₂ evolution ($CE_{a,\text{OER}}$) as well as the cathodic CE for H₂ evolution ($CE_{c,\text{HER}}$) generally increased over the experimental range of j , and approximately 70% of CEs were observed for j values greater than 300 A m⁻². It should be noted that the $CE_{c,\text{HER}}$ and $CE_{a,\text{OER}}$ given here are nominal values estimated from the collected and analyzed gaseous products. In Fig. 4(c), the observed $CE_{c,\text{HER}}$ was found to be smaller than $CE_{a,\text{OER}}$ by 7% in maximum at E_a of 1.8 V; *i.e.*, the molar ratio of H₂ to O₂ (X_H/X_O) in the headspace was slightly lower than stoichiometric ratio of 2. If we assume that other reaction by-products than the reactive oxygen species (H₂O₂, HO₂, O₃, •OH, and *et cetera*) should be negligible in the NaClO₄ system, the CE of HER should be equal or greater than that of OER [44,45]. Therefore, the slight discrepancy between the anodic and cathodic CE might be ascribed to bubbles attached to the electrodes module or dis-

Table 1
Reactions of primary importance in single compartment wastewater electrolysis cell.

Phase	ID	Representative Reaction	E° (V)
Anodic	A1	OER: $2\text{H}_2\text{O} \rightarrow \text{O}_2 + 4\text{H}^+ + 4\text{e}^-$	−1.23
	A2	CIER: $2\text{Cl}^- \rightarrow \text{Cl}_2 + 2\text{e}^-$	−1.36
	A3	CIOER: $3\text{ClO}^- + 3/2\text{H}_2\text{O} \rightarrow \text{ClO}_3^- + 2\text{Cl}^- + 3\text{H}^+ + 3/4\text{O}_2 + 3\text{e}^-$	−1.14
Cathodic	C1	HER: $2\text{H}^+ + 2\text{e}^- \rightarrow \text{H}_2$	0
	C2	CIRR: $\text{ClO}^- + \text{H}_2\text{O} + 2\text{e}^- \rightarrow \text{Cl}^- + 2\text{OH}^-$	0.81
	C3	ORR (4e [−]): $\text{O}_2 + 4\text{H}^+ + 4\text{e}^- \rightarrow \text{H}_2\text{O}$	1.23
	C4	ORR (2e [−]): $\text{O}_2 + 2\text{H}^+ + 2\text{e}^- \rightarrow \text{H}_2\text{O}_2$	0.70
	C5	$\text{H}_2\text{O}_2 + \text{Cl}^- \rightarrow \text{ClO}^- + \text{H}_2\text{O}$	–
Homogeneous	H1	$\text{Cl}_2 + \text{H}_2\text{O} \leftrightarrow \text{HOCl} + \text{Cl}^- + \text{H}^+$	–
	H2	$\text{HOCl} \leftrightarrow \text{OCl}^- + \text{H}^+$	–

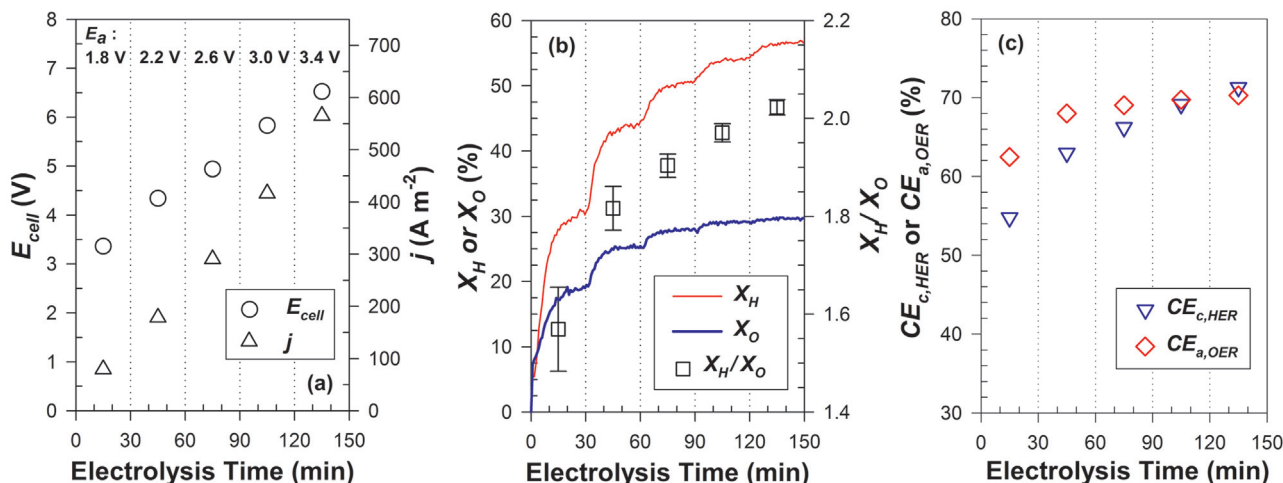


Fig. 4. Characteristics of collected gas products from a single compartment electrolysis cell with $\text{BiO}_x/\text{TiO}_2$ anode and AISI 304 cathode in 50 mM NaClO_4 solutions under stepwise increments of applied anodic potential: (a) cell voltage and current density, (b) fractions of H_2 and O_2 in gas products, and (c) apparent current efficiency for H_2 and O_2 evolution.

persed in the electrolyte, whose relative contributions to CE would be mitigated as the rate of electrolysis increases.

In the NaClO_4 solutions in the absence of other redox active species aside from those generated from water, the losses in CEs could occur either from reduction of dissolved O_2 or oxidation of dissolved H_2 . However, H_2 oxidation on metal oxide anode surface could be ruled out especially in the potential window of OER, owing to inhibitions by (higher) oxides [45]. Dissolved O_2 can be reduced to water (C3 in Table 1) on cathode to form the superoxide radical, hydrogen peroxide, and hydroxyl radical as reaction intermediates presumably in surface-bound forms [46]. The cathodic potentials (−1.5 to −3.0 V), were below the redox potential of O_2/HO_2^- couple (−0.54 V at pH 7), and enough to initiate the oxygen reduction reaction (ORR). In case of AISI 304 cathode, surficial Ni rather than Fe may provide the active site for the ORR [47]. It is well established that the ORR is limited by diffusion of the dissolved O_2 to the electrode surface [45]. In this regard, both theoretical and experimental studies have shown that the efficiency of electrolytic gas products formation increases nonlinearly with increasing j in undivided electrolysis cells for both O_2 [44,48,49] and H_2 [44,48–52]. Although a rise in the micro-convective mass transfer coefficient [48] and a decrease in diffusion layer thickness [45,50] are expected, an increasing j should allow for the charge-transfer controlled HER to dominate the diffusion controlled ORR. In addition, an increasing j may result in a greater coverage of electrode surfaces by bubbles [48,49,52–54] and vicinal supersaturation concentration of H_2 and O_2 [49,55], in turn enhances the mass transport of dissolved products into the gas phase (rising bubbles). Nonetheless, the effect of

j could become insignificant when the surface coverage of bubbles and the supersaturation concentration reach their maximum limits.

3.2.2. Free chlorine generation in dilute chloride solutions

At a sufficiently large anodic potential bias, Cl^- is electrochemically oxidized to produce molecular chlorine (Cl_2 , A2 in Table 1) and it is subsequently hydrolyzed (HOCl and ClO^- , H1–2 in Table 1) to give free chlorine (FC) as a collective term. Fig. 5 shows the specific rate ($r_{a,\text{FC}}$) and anodic CE ($\text{CE}_{a,\text{FC}}$) for FC generation, or the chlorine evolution reaction (CIER), on the multi-junction anode in NaCl solutions (10 to 50 mM) at variable cell voltages. Concentrations of FC were appreciable when E_a exceeds 1.5 V owing to the iR drop, though the standard reduction potential of Cl_2/Cl^- couple is 1.36 V. The $r_{a,\text{FC}}$ monotonically increased along with either $[\text{Cl}^-]$ or E_{cell} , as readily expected. At each $[\text{Cl}^-]$ level, the $\text{CE}_{a,\text{CIER}}$ as a function of E_{cell} followed a general saturation trend as described previously [29]. The initial increase in $\text{CE}_{a,\text{CIER}}$ with E_a is consistent with a lower Tafel slope for the CIER than for the OER [56], which is in turn, inversely proportional to the charge transfer coefficient. At E_{cell} greater than 3.5 V, the $\text{CE}_{a,\text{CIER}}$ values reached a plateau and showed marginal variations with E_{cell} in the range from 25 to 30% for 30 and 50 mM NaCl. As the E_{cell} and iR -compensated anodic potential increase under Nernstian equilibrium, there will be an increased level of transient binding of the surficial active sites by the higher valence-state oxide. The kinetic contributions of the higher oxide in the OER and the CIER are in chemical reaction limited regime and thus there is a negligible influence of E_{cell} [8]. In addition, a diffusion limitation for CIER would also limit further increase of $\text{CE}_{a,\text{CIER}}$, as in the increasing $\text{CE}_{c,\text{HER}}$ with j observed in Fig. 4.

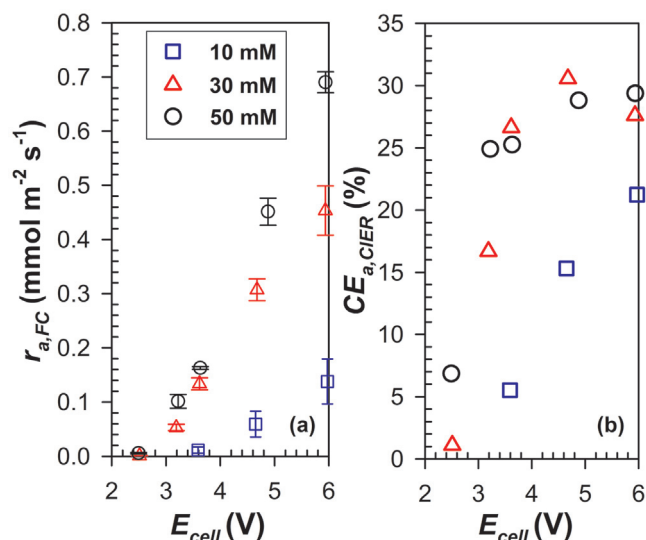


Fig. 5. The efficacy of free chlorine generation in terms of (a) rate and (b) current efficiency for a single compartment electrolysis cell with BiO_x/TiO₂ anode and AISI 304 cathode in NaCl solutions with variable concentrations.

The electrochemical relay effects of the FC in undivided electrolysis cells have been often noted [50,51,57,58], where chlorine reduction reaction (CIRR) on cathodes such as stainless steel [10,12,15–17,20] reduces the CE both for CIER and HER. Although the active components of stainless steel responsible for the FC reduction are unknown, it has been proposed to be inhibited by surficial metal oxides or hydroxides [50]. The hypochlorite ion is most likely the initiator of the CIRR (C2 in Table 1), considering the local high pH near the cathode surface [16,57]. In order to assess the interference of CIRR in these experimental sets, a nonlinear relationship [50,51] was employed to estimate thickness of Nernst diffusion layer as a function of j , while the diffusion coefficient of ClO[−] was assumed to be in the order of 10^{−5} cm² s^{−1}. These rough calculations suggested insignificant rates of FC reduction within 1.1–3.8% of $r_{a,FC}$ values, since the bulk concentrations of FC were mostly lower than 1 mM. Anodic chlorate formation due to the oxidation of FC (CIOER, A3 in Table 1) is known as additional parasitic side reaction [8,9,51,57,58]. However, subsequent analysis confirmed that a negligible concentration of chlorate was produced over the short reaction times. As a consequence, the results shown in Fig. 5 should give reasonable estimates for the FC evolution efficiency for near ideal cases; i.e., in absence of side reactions, a linear correlation (CE_{a,CIER} of 0.28 on average) of $r_{a,FC}$ with j is expected when E_{cell} and [Cl[−]] are not less than 3.5 V and 30 mM, respectively.

3.2.3. Effects of chloride ions and organics on molecular hydrogen generation

The HER has been reported to be suppressed in the presence of chloride ion when compared to electrochemically inert electrolyte components (e.g., SO₄^{2−}, ClO₄[−]), due to the CIRR [12,15,16]. More evident examples have been presented by Park et al. [10], where an injection of free chlorine quenchers during electrolysis of NaCl solutions resulted in sharp increases of CE_{c,HER}. The CIRR would compete both with the cathodic HER (for electrons) and the homogeneous reactions of pollutants abatement (for FC). With this consideration in mind, the concentration of FC would be a primary determinant of CE_{c,HER} in WEC, which is in-turn affected by the oxidizable components (e.g., represented by chemical or biochemical oxygen demand) present in wastewater. The dynamic variations in CE_{c,HER} and CE_{a,OER} along with redox transformations of chlorine species are illustrated in Fig. 6. In a batch reactor electrolysis in a solution of 50 mM NaCl at E_a of 3 V NHE (E_{cell} to be 5.2 V on average),

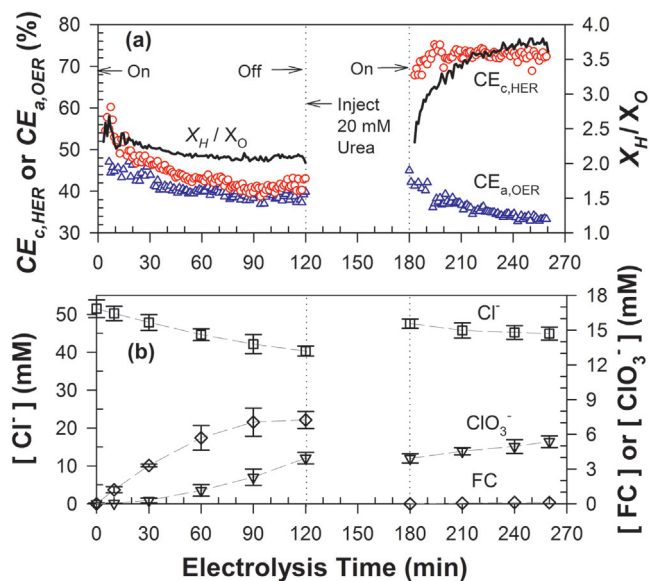


Fig. 6. Variations in (a) current efficiency of H₂ and O₂ generation (magnitudes and ratio), together with (b) concentrations of Cl[−], free chlorine (FC), and ClO₃[−] in aqueous phase during a single compartment electrolysis initiated in 50 mM NaCl solution at 3.0 V NHE of anodic potential. 20 mM of urea was injected after 2 h to quench the FC during 1 h of open circuit.

the j values (350 A m^{−2} on average) were sufficiently high so that the effects of j on CE_{c,HER} were of less importance (*vide supra*). The initial CE_{c,HER} estimates were below those in NaClO₄ solution and they monotonically decreased to 0.4 corresponding to the increase in the FC concentration. Therefore, the timing and duration of sampling affect the measurement of CE_{c,HER} in variable NaCl solutions, which explains the wide variation of CE_{c,HER} in previous reports (30–60%) [14,20,21] using similar experimental configurations. The evolution of FC reached saturation at approximately 7 mM due to CIRR and CIOER [8]. The CE_{a,OER} was somewhat lower than CE_{c,HER} at the beginning of electrolysis and then, after some time, became almost superimposable (stoichiometric) as also indicated by the continuous decrease in X_H/X_O from 2.5 to 2.1.

For a reaction duration from 90 to 120 min, CE_{c,HER} and CE_{a,OER} values were averaged to 0.41 and 0.39, respectively. For the same time period, the apparent anodic CE for CIER and CIOER (3 electron oxidation from FC) were estimated to be <1% and 9.8%, respectively. If we assume a value of 0.3 for CE_{c,ORR} as in NaClO₄ solutions (Fig. 4 at comparable values of j), the cathodic charge valence equation (CE_{c,HER} + CE_{c,ORR} + CE_{c,CIRR} = 1) gave CE_{c,CIRR} of 0.29. However, this estimate was close to the CE_{a,CIER} value observed in Fig. 5 (0.28) and, thus, could not account for the CIOER in the mass balance of FC. In this regard, we argue that a shift in ORR pathway by chloride ions takes place that may resolve this discrepancy with a decrease in CE_{c,ORR}. The classically accepted theory on electrochemical ORR suggests the surface-bound hydrogen peroxide as the intermediate with a relatively long life, so that the ORR with 2 electrons transfer (C4 in Table 1) can be often distinguished from that with 4 electrons transfer (C3 in Table 1) [46]. Schmidt et al. [59] would be a good example of the situation where the chloride ions with a concentration as small as 0.1 mM could retard oxide formation, promoting H₂O₂ formation rather than complete reduction of O₂. Based on the redox potential of H₂O₂ and FC, the surficial peroxide would function effectively to produce FC *via* reaction C5 in Table 1. Although the reaction of Cl[−] with H₂O₂ itself would be kinetically sluggish, reductive decomposition products of H₂O₂ (such as •OH) would effectively mediate the reaction C5 [10]. In this reaction regime, the overall ORR sequences partially accept electrons from chloride ions rather than from the cathode, which in-turn decrease the

$CE_{c,ORR}$ at a given diffusion rate of O_2 towards the cathode. From a macroscopic perspective, the amount of electrons gathered from formation of FC and ClO_3^- in aqueous phase ($\sim 10\%$) was greater than the excess electrons given to the gas phase ($CE_{c,HER} - CE_{a,OER}$, 2%). In the postulated ORR driven FC generation scheme, the dissolved O_2 would accept the surplus electrons from the aqueous phase.

An enhancement of $CE_{c,HER}$ with the addition of electron donating substances in bulk aqueous phase was obvious based on the impact of an injection of urea after 2 h of electrolysis. The concentration of urea (20 mM) injected should be enough to dramatically lower the FC during the open circuit period of 1 h. When the anodic bias was applied again, the residual urea together with degradation intermediates should have been involved in facile reactions to suppress the anodically generated FC. Given this condition, the $CE_{c,HER}$ was actually elevated to 75%, which was even greater than in Na_2SO_4 solutions. The enhancement in H_2 production in the presence of chloride ion (and oxidizable organics) than when they are absent has been observed previously [16], even though a satisfactory mechanism was not provided. These observations provide further evidence for a shift in ORR pathway by chloride ions as well. In addition, the *in-situ* generation of free chlorine in the WEC would be desirable for H_2 production purposes, when compared to a multi-component system with external FC generation and subsequent wastewater treatment in a separate vessel.

3.3. Current and energy efficiency of H_2 production in wastewater electrolysis cell

3.3.1. Current efficiency in urea solutions

The evolution of H_2 in a WEC was more thoroughly probed using urea as the model organic compound. The urea is the dominant source of nitrogen in domestic and toilet wastewater. In addition, its simple molecular structure allows for an easy quantification of the reaction/degradation products; *i.e.*, the primary gaseous degradation products of urea, N_2 and CO_2 , do not involve mass fragments overlapping with H_2 and O_2 . Fig. 7 illustrates the evolution of H_2 and O_2 in a batch WEC experiment with model wastewater (2.5 g L^{-1} urea with 50 mM NaCl) together with the variations in major nitrogen and chlorine species in aqueous phase. Urea degradation via electrochemically generated FC was apparent in the decay profile of the TN concentration. From a mechanistic perspective as we discussed previously [29], combined chlorine species such as chloramides (chlorinated urea) and chloramines are the major reaction intermediates, while N_2 , CO_2 , and NO_3^- are the final products of a homogeneous reaction network. The mass fragmentation patterns of the headspace gases also indicated that N_2 and CO_2 were the primary constituents besides H_2 and O_2 , whose molar fractions varied considerably during the course of electrolysis. A control experiment showed marginal degradation of urea in 50 mM $NaClO_4$ solutions, implying that the heterogeneous reactive oxygen species would play a minor role in pollutants oxidation for the multi-junction BiO_x/TiO_2 anode [8,9,29].

The classical breakpoint chlorination mechanism for the removal of nitrogen species during chlorination provides a reasonable interpretation of the variation in total chlorine (TCI), in which the shifts in aqueous and gaseous compositions indicated the apparent breakpoint after about 3.5 h. The FC was not measurable (data not shown) until the breakpoint and subsequently increased up to 6.6 mM along with the complete consumption of all electron donors. The build-up of FC coincided with an accelerated accumulation of ClO_3^- after the breakpoint. Direct experimental knowledge was obtained that a dramatic change in H_2 generation occurs after the breakpoint. The $CE_{c,HER}$ showed marginal variation near 75% which was sharply tapered off after the breakpoint. The X_H in the gaseous products monotonically rose until the breakpoint,

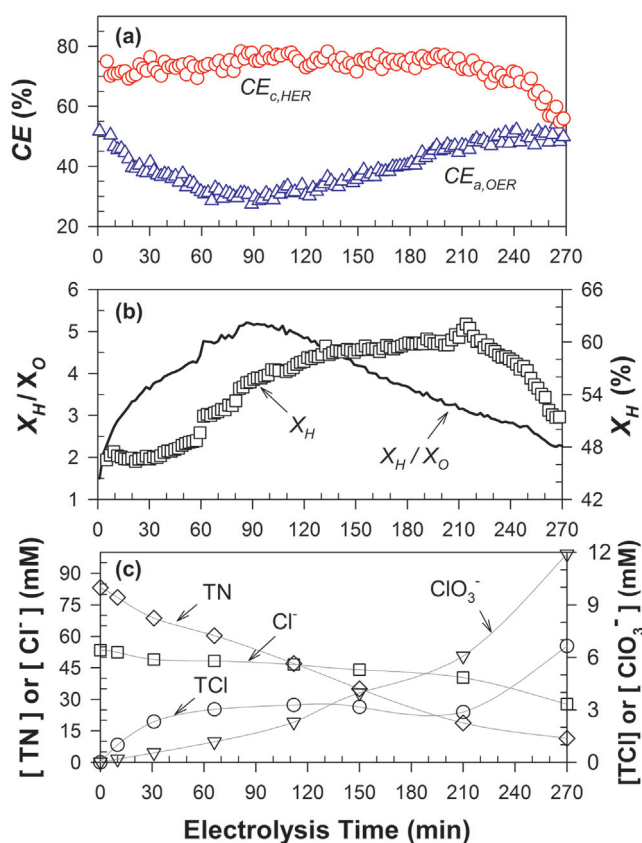


Fig. 7. Variations in (a) current efficiency of H_2 and O_2 generation, (b) volumetric fraction of H_2 and O_2 in gas phase, and (c) concentrations of total nitrogen (TN), total chlorine (TCI), Cl^- , and ClO_3^- in aqueous phase during a wastewater electrolysis cell experiment initiated in 2.5 g L^{-1} urea with 50 mM NaCl solution at 3.0 V NHE of anodic potential.

together with decreasing formations of N_2 and CO_2 under a pseudo first-order kinetic regime [29]. The strong relationship between $CE_{c,HER}$ and the concentration of FC is consistent with our interpretation that the predominant electron acceptors interfering with HER are O_2 and FC. From a water treatment standpoint, the ratio of chloride ion to oxidizable substances was proven to determine the anodic CE for chemical contaminant removal [8]. However, the concentrations of FC quenching substances (urea and its degradation intermediates in this case) are of minor concern for $CE_{c,HER}$ provided that FC is in pseudo steady-state level. The anions NO_3^- and ClO_3^- were found to be stable reaction products, since their conversions were negligible during separate electrolysis of 50 mM $NaNO_3$ and $NaClO_3$ solutions (data not shown). Considering the redox potential of the NO_3^-/NO_2^- (0.42 V at pH 7) and the ClO_3^-/ClO_2^- couples, the reduction of these anions should be kinetically limited on a AISI 304 cathode.

The $CE_{a,OER}$ appeared to decrease from 0.5 to 0.3 for the first 1.5 h and then increased back to the initial value during further electrolysis. The initial reduction in $CE_{a,OER}$ (also observed during the second electrolysis in Fig. 6) was inverted roughly when the maximum plateau of TCI was achieved. This observation illustrates the potential involvement of dissolved oxygen in the formation of various reaction intermediates from urea, albeit no direct evidence is available in literature. It has been reported that the $CE_{a,OER}$ is also influenced by the concentration of FC via O_2 liberation during the CLOER sequences [10,50], though the sensitivity is not as high as $CE_{c,HER}$ [51]. The quasi-steady-state $CE_{c,HER}$ values observed until the breakpoint is reached indicated that the variations in $CE_{a,OER}$ by more than 0.2 should not influence the rate of ORR, which depends

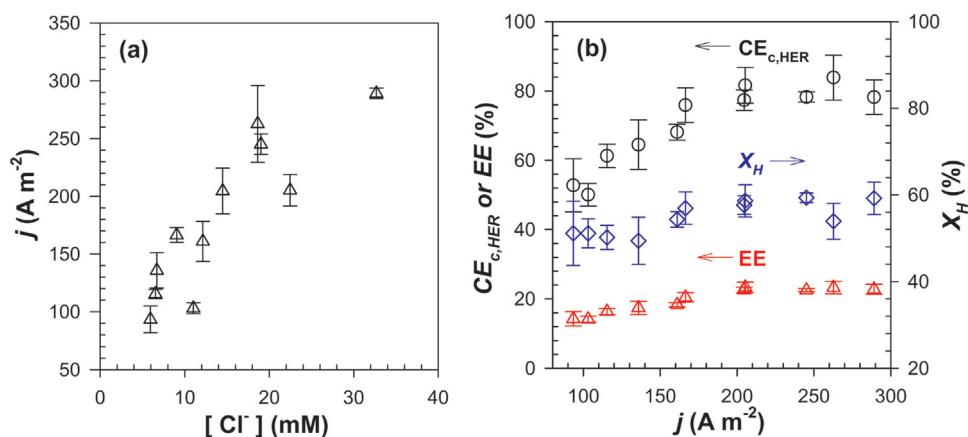


Fig. 8. Molecular hydrogen production from wastewater electrolysis cell experiments with real wastewater samples at 3.0 V NHE of anodic potential: (a) current density for wastewater samples with variable combinations of Cl^- concentrations together with (b) volumetric fraction of H_2 , current and energy efficiency of H_2 generation.

Table 2

Initial concentrations of chemical oxygen demand (COD) and chloride ions for wastewater samples employed in wastewater electrolysis cell experiments and corresponding current density (j) on average.

Source	[COD] ₀ (mg L ⁻¹)	[Cl ⁻] ₀ (mM)	j (A m ⁻²)
Domestic	61.0	32.7	289
Wastewater + 50 mM NaCl	102	22.5	205
	128	12.1	161
	139	11.0	103
Stored	110	18.6	263
Urine + Domestic	266	5.94	93.4
Wastewater	304	6.54	115
	367	6.70	136
	431	9.04	166
	621	14.5	205
	794	19.0	245

on the dissolved O_2 concentration at supersaturation. The CIER and CIOER again would serve as the main scavenging reaction of OER, leading to non-stoichiometric water splitting as shown by X_H/X_O in Fig. 7b.

3.3.2. Current and energy efficiency in variable types of real wastewater

Fig. 8 shows major figures of merit for H_2 production as functions of j in WEC experiments with real wastewater. As illustrated in Table 2, variable mixing ratios among 50 mM NaCl solutions, domestic wastewater, and stored urine allowed preparation of wastewater samples with initial $[Cl^-]$ and [COD] ranging from 5.9 to 32.7 mM and 60 to 790 mg L⁻¹, respectively. The electrical conductivity ranged from 1.4 to 5.2 mS cm⁻¹ increasing nonlinearly with $[Cl^-]$, as illustrated in Fig. 3. During the gas collection period of 30 min, the concentration of FC was below the detection limit so that the influence of CIRR on $CE_{c,HER}$ could be excluded in our estimates. The CE and EE for H_2 generation varied as a function of j ; 50% and 13% at about 100 A m⁻² of j which increased up to 85% and 23% under j values from 200 to 300 A m⁻². Considering the wide variety in the wastewater composition from various sources, it is clear that the current density is the predominant factor determining the $CE_{c,HER}$. As for COD reduction, the molar ratio of chloride ions to the various reductants and the reactivity of FC toward specific reductants or oxidizable organic and inorganic compounds have been identified as the primary determinants of the anodic CE [8,9]. In contrast, the quantity of electron donating species in terms of COD gave a tenuous relation to the measured $CE_{c,HER}$. The pseudo first-order decay constants of COD varied from 2.38×10^2 to 2.95×10^3 s⁻¹ for the samples giving comparable $CE_{c,HER}$ values

near 0.8. In our experimental scheme under the constant anodic potential of 3.0 V NHE, the j values increased with an increase in $[Cl^-]$ and electrical conductivity (Fig. 8(a)). Consequently, the binary functions of the WEC (water treatment combined with H_2 generation) would be enhanced if the wastewater had a high salinity wastewater for which the electrical conductivity might reach 10 mS cm⁻¹ for some industrial wastewater. One can also imagine adding seawater or brine water from desalination as a measure to enhance the wastewater conductivity for small-scale facilities in coastal area.

Previous studies reported $CE_{c,HER}$ values scattered over the range of 40–90% [8,9,17,20] and these varied results can be understood in terms of the impact of j on the measure parameters, as demonstrated in this study. In addition, data compilation even at a given j needs careful interpretation since the hydrodynamic characteristics under variable electrolysis cell configurations could affect the kinetics of ORR. The specific composition array of oxidizable substrates was found to be a minor factor influencing the value of $CE_{c,HER}$ as long as keeping the FC in pseudo steady-state. However, the potential participation of wastewater constituents (or degradation products) to the cathodic reactions cannot be ruled out completely. In Fig. 8(b), $CE_{c,HER}$ values on the plateau (~0.8) were even greater than in the case of urea solutions (~0.75) whose degradation intermediates (chloramines or chloramides) are suspected to accept electrons from the cathode. Total chlorine concentrations during electrolysis of actual wastewater were always lower than 0.5 mM, whereas values as high as 3 mM were observed during the breakpoint chlorination of urea (Fig. 7(c)). The reduction potential of monochloramine, which accepts 2 electrons to give ammonium and chloride, was reported to be 1.1 V NHE at pH 7 [60]. In contrast to urea, which is essentially non-reactive with H_2O_2 in circum-neutral pH, the array of organics in real wastewater matrix might in-part quench the peroxy intermediates in the ORR sequences, in the same manner the chloride ions reduce the $CE_{c,ORR}$.

The EE of the WEC appeared to be no greater than 23%, far lower than commercialized electrolytic H_2 production methods such as alkaline and PEM electrolysis units. Voltage efficiency is another parameter that is used to assess electrolytic systems; the voltage efficiency is defined as the ratio of reversible cell voltage for the water splitting (1.23 V) to the applied cell voltage [1]. As the voltage efficiency approaches the EE, the $CE_{c,HER}$ approaches unity. Voltage losses are caused by activation overvoltage on the electrodes, ohmic solution resistance, and mass transport resistance associated with diffusion layer and surface-attached bubbles [1,4]. When compared to a typical alkaline electrolysis unit, the solution resistance should contribute most of intensive energy loss in WEC even

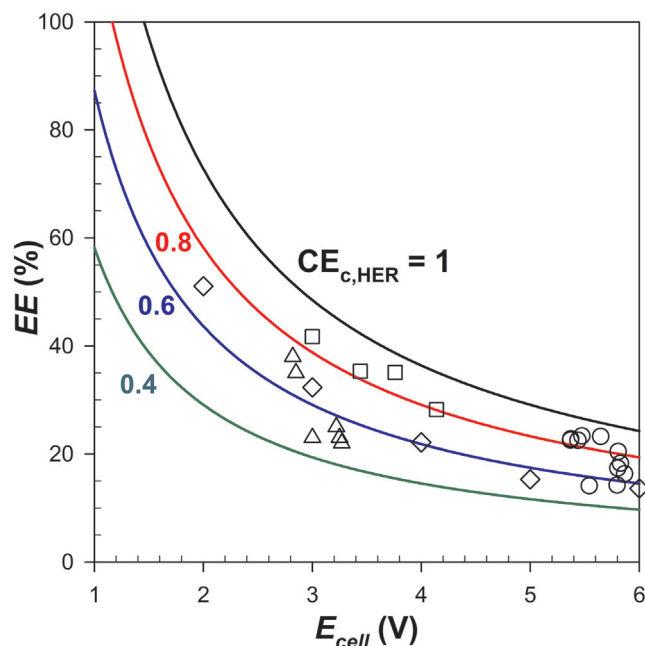


Fig. 9. Energy efficiency of H₂ generation as functions of cell voltage referenced with (solid lines) theoretical calculation for variable current efficiency and reported values in literature: (□) Ref. [17], (◇) Ref. [21], (Δ) Ref. [20], and (○) this study.

though the absence of membrane alleviates the mass transfer resistance. A rearrangement of the equation for EE (Eq. (2)) essentially gives a formulation in terms of voltage efficiency multiplied by the $CE_{c,HER}$.

$$EE = \frac{HHV \times Q_H}{E_{cell} \times i} = \frac{HHV}{E_{cell}} \times \frac{CE_{c,HER}}{nF} \quad (3)$$

The EE values obtained herein are plotted against E_{cell} in Fig. 9 and compared directly to the reported values extracted from the literature that were obtained using synthetic and real wastewater as the primary electron donors [17,20,21]. The data from literature was chosen when the E_{cell} was sufficiently greater than the thermodynamic potential of water splitting so that the primary redox reactions presented in Table 1 would be feasible. The substantial variations in the values of EE can be readily interpreted by an inverse proportionality to the E_{cell} . The EE intrinsically should increase with a decreasing E_{cell} , which reduces the energy loss due to ohmic resistance [1]. The relationship given in Eq. (3) predicts a reduced impact of $CE_{c,HER}$ on EE as the E_{cell} increases. Given the data reported herein, the increase in $CE_{c,HER}$ by 33% as a function of j corresponded to a 9% difference in EE since E_{cell} only ranged between 5 and 6 V. Thus, the dependence of EE on j is less significant than for $CE_{c,HER}$ as shown in Fig. 8(b).

The strict dependency of EE on the E_{cell} indicates that an improvement in EE should be viable. For example, higher EE values up to 52% have been reported at E_{cell} settings near 2 V during the electrolysis of municipal wastewater with external chloride ions [21]. However, a lower E_{cell} should decrease j as depicted in linear sweep voltammetry (Fig. 3), which results in a reduced $CE_{c,HER}$ at j values less than 200 A m⁻² as shown in Fig. 8. Therefore, a reduction in E_{cell} would not always yield a larger EE, considering that the impact of $CE_{c,HER}$ on EE is more significant at lower E_{cell} . In case of electrolysis of wastewater for which [COD]₀ = 105 mg L⁻¹ and [Cl⁻] = 22.5 mM at an E_{cell} of 4.0 V, the EE was determined to be 16% which is far smaller than at an E_{cell} of 5.5 V (EE = 23%) due to corresponding reduction in $CE_{c,HER}$ (~45%). In this regard, employment of a high-salinity wastewater (e.g., landfill leachate, food waste) or external addition of chloride salts would provide a strategy to

enhance EE by reducing E_{cell} without a corresponding reduction in $CE_{c,HER}$. Additional research is necessary to determine an optimal E_{cell} in the trade-off relationship between EE and $CE_{c,HER}$, which is dependent on the conductivity of the wastewater to be treated.

The H₂ production rates per unit volume of WEC were measured over the range from 0.9 to 4.2 mol H₂ L⁻¹ h⁻¹. In order to run a 5 kW fuel cell sufficient for a residential power source, the working volume could be reduced to 30 L, which is orders of magnitude smaller than other H₂ production methods from wastewater such as microbial fuel (electrolysis) cells or photolysis [3]. Nonetheless, the purity of the mixed-state H₂ was 60% at a maximum, which constrains a direct utilization of the gas produced to run internal combustion engines whose energy conversion efficiency is below 40% [61]. Although a thorough analysis of the gases products were not quantified for real wastewater samples, the impurities will include O₂, H₂O, N₂, and CO₂, as shown in the case of urea as a substrate. It should be possible to use a PEM or solid-state fuel cell to convert the gaseous product into electricity in combination with i) a gas separating membrane (diaphragm) inside the WEC, ii) membrane-based H₂ purification at the gas outlet, or iii) via high temperature operation of a solid acid electrolyte designed to work using H₂ mixed with impurities.

In WECs, the overall current generation is usually governed by anodic reactions so that the type of cathode material might be of less importance for H₂ production, especially under the diffusion controlled regime for the ORR. However, enhancement of $CE_{c,HER}$ can be achieved using HER catalysts with a reduced selectivity toward the ORR. Although the volcano plots for HER and ORR largely resemble with each other for various transition metals [62], binary or ternary architectures may be capable of tuning the binding energies to O and H. Since reactions involving O₂ nullify the redox network for pollutants abatement and molecular hydrogen production, increasing the anodic selectivity to ClER would provide another strategy to enhance the $CE_{c,HER}$. In this regard, we have recently developed heterojunction anodes with surface enriched with crystalline TiO₂ that yield elevated $CE_{a,ClER}$ values in dilute chloride solutions, when compared to a IrO₂-based anode [23]. In spite of the reduced current generation observed along with the increase in surficial crystallinity, an enhancement in EE might be feasible by mitigating the electron shuttling effects owing to O₂ ($CE_{a,ORR}$ and $CE_{c,ORR}$).

4. Conclusions

In this study, we determined the current (CE) and energy (EE) efficiencies of molecular hydrogen production in a single compartment wastewater electrolysis cell (WEC), which consists of BiO_x/TiO₂ anode, AISI 304 stainless steel cathode and wastewater with electrical conductivity less than 5.50 mS cm⁻¹. Electroactive anodes were prepared in a multi-junction architecture with surface mixed oxide layer of Ti and Bi, whose quasi-amorphous structure provide unsaturated active sites with structural flexibility for OER intermediates formation. The primary effects of operational parameters such as current density (j , <500 A m⁻²), cell voltage (E_{cell} , <6 V) and wastewater compositions are summarized as follows:

1. The CE for anodic free chlorine (FC) generation increased with [Cl⁻] and anodic potential with saturation behavior up to ~0.3. Production of O₂ and ClO₃⁻ were primary side reactions taking place on the anode, while reduction of O₂ and FC interfere with cathodic H₂ production. The CE for H₂ production ($CE_{c,HER}$) increased with an increasing j owing to diffusion limited nature of the scavenging reactions.
2. A presence of Cl⁻ exerts a positive effect on $CE_{c,HER}$ by increasing j at a given E_{cell} and presumably quenching the intermediates

(surface peroxide) in the O_2 reduction sequence. The chemical oxygen demand (primarily organic reductants) in wastewater readily exhausted the FC and elevated $CE_{c,HER}$. The EE for H_2 production nonlinearly decreased with an increasing E_{cell} .

3. The $CE_{c,HER}$ and EE for H_2 production from real wastewater approached 0.8 and 0.23 at j greater than 200 A m^{-2} . The primary findings of this study suggest that the WEC is more suitable process for a high-salinity wastewater.

Acknowledgments

The authors would like to acknowledge the financial support of the Bill and Melinda Gates Foundation (BMGF RTTC Grant OPP1111246). This work was financially supported in part by the Nano Material Technology Development Program through the National Research Foundation of Korea (NRF-2016M3A7B4908161) and Korea Ministry of Environment as “Global Top Project” (Project No.: 2016002190003).

References

- [1] K. Zeng, D.K. Zhang, Recent progress in alkaline water electrolysis for hydrogen production and applications, *Prog. Energy Combust. Sci.* 36 (2010) 307–326.
- [2] I. Dincer, C. Acar, Review and evaluation of hydrogen production methods for better sustainability, *Int. J. Hydrogen Energy* 40 (2015) 11094–11111.
- [3] J.D. Holladay, J. Hu, D.L. King, Y. Wang, An overview of hydrogen production technologies, *Catal. Today* 139 (2009) 244–260.
- [4] M. Carmo, D.L. Fritz, J. Merge, D. Stolten, A comprehensive review on PEM water electrolysis, *Int. J. Hydrogen Energy* 38 (2013) 4901–4934.
- [5] M. Ni, M.K.H. Leung, D.Y.C. Leung, Technological development of hydrogen production by solid oxide electrolyzer cell (SOEC), *Int. J. Hydrogen Energy* 33 (2008) 2337–2354.
- [6] G. Gahleitner, Hydrogen from renewable electricity: an international review of power-to-gas pilot plants for stationary applications, *Int. J. Hydrogen Energy* 38 (2013) 2039–2061.
- [7] U.S. DOE, Multi-Year Research, Development, and Demonstration Plan: Planned program activities for 2011–2020, U.S. Department of Energy, http://energy.gov/sites/prod/files/2015/06/f23/fcto_myrdp_production.pdf, Accessed on 26.02.16.
- [8] K. Cho, D. Kwon, M.R. Hoffmann, Electrochemical treatment of human waste coupled with molecular hydrogen production, *RSC Adv.* 4 (2014) 4596–4608.
- [9] K. Cho, Y. Qu, D. Kwon, H. Zhang, C.A. Cid, A. Aryanfar, M.R. Hoffmann, Effects of anodic potential and chloride ion on overall reactivity in electrochemical reactors designed for solar-powered wastewater treatment, *Environ. Sci. Technol.* 48 (2014) 2377–2384.
- [10] H. Park, C.D. Vecitis, M.R. Hoffmann, Electrochemical water splitting coupled with organic compound oxidation: the role of active chlorine species, *J. Phys. Chem. C* 113 (2009) 7935–7945.
- [11] P.L. McCarty, J. Bae, J. Kim, Domestic wastewater treatment as a net energy producer—can this be achieved? *Environ. Sci. Technol.* 45 (2011) 7100–7106.
- [12] H. Park, C.D. Vecitis, W. Choi, O. Weres, M.R. Hoffmann, Solar-powered production of molecular hydrogen from water, *J. Phys. Chem. C* 112 (2008) 885–889.
- [13] M. Panizza, G. Cerisola, Direct and mediated anodic oxidation of organic pollutants, *Chem. Rev.* 109 (2009) 6541–6569.
- [14] H. Park, C.D. Vecitis, M.R. Hoffmann, Solar-powered electrochemical oxidation of organic compounds coupled with the cathodic production of molecular hydrogen, *J. Phys. Chem. A* 112 (2008) 7616–7626.
- [15] J. Kim, W.J.K. Choi, J. Choi, M.R. Hoffmann, H. Park, Electrolysis of urea and urine for solar hydrogen, *Catal. Today* 199 (2013) 2–7.
- [16] S. Kim, S.K. Choi, B.Y. Yoon, S.K. Lim, H. Park, Effects of electrolyte on the electrocatalytic activities of RuO_2/Ti and $Sb-SnO_2/Ti$ anodes for water treatment, *Appl. Catal. B-Environ.* 97 (2010) 135–141.
- [17] J. Kim, D. Kwon, K. Kim, M.R. Hoffmann, Electrochemical production of hydrogen coupled with the oxidation of arsenite, *Environ. Sci. Technol.* 48 (2014) 2059–2066.
- [18] J.Y. Jiang, M. Chang, P. Pan, Simultaneous hydrogen production and electrochemical oxidation of organics using boron-doped diamond electrodes, *Environ. Sci. Technol.* 42 (2008) 3059–3063.
- [19] W. Ma, Z.H. Cheng, Z.X. Gao, R. Wang, B.D. Wang, Q. Sun, Study of hydrogen gas production coupled with phenol electrochemical oxidation degradation at different stages, *Chem. Eng. J.* 241 (2014) 167–174.
- [20] J. Choi, Y. Qu, M.R. Hoffmann, SnO_2 , IrO_2 , Ta_2O_5 , Bi_2O_3 , and TiO_2 nanoparticle anodes: electrochemical oxidation coupled with the cathodic reduction of water to yield molecular H_2 , *J. Nanopart. Res.* 14 (2012).
- [21] H. Park, K.H. Choo, H.S. Park, J. Choi, M.R. Hoffmann, Electrochemical oxidation and microfiltration of municipal wastewater with simultaneous hydrogen production: influence of organic and particulate matter, *Chem. Eng. J.* 215 (2013) 802–810.
- [22] J.Y. Jiang, J.L. Hu, M.X. Cui, H. Tian, Integration of hydrogen production and waste heat recovery in electrochemical wastewater treatment, *Renew. Energy* 43 (2012) 179–182.
- [23] K. Cho, M.R. Hoffmann, $Bi_xTi_{1-x}O_2$ functionalized heterojunction anode with an enhanced reactive chlorine generation efficiency in dilute aqueous solutions, *Chem. Mater.* 27 (2015) 2224–2233.
- [24] H. Liu, A. Vajpayee, C.D. Vecitis, Bismuth-doped tin oxide-coated carbon nanotube network: improved anode stability and efficiency for flow-through organic electrooxidation, *ACS Appl. Mater. Interfaces* 5 (2013) 10054–10066.
- [25] H. Park, A. Bak, Y.Y. Ahn, J. Choi, M.R. Hoffmann, Photoelectrochemical performance of multi-layered BiO_x-TiO_2/Ti electrodes for degradation of phenol and production of molecular hydrogen in water, *J. Hazard. Mater.* 211 (2012) 47–54.
- [26] O. Weres, H.E. O'Donnell, Multilayer Oxide Coated Valve Metal Electrode for Water Purification, US 6589405 B2, 2003.
- [27] O. Weres, Electrode with Surface Comprising Oxides of Titanium and Bismuth and Water Purification Process Using This Electrode, US 7494583 B2, 2009.
- [28] A.J. Bard, L.R. Faulkner, *Electrochemical Methods: Fundamentals and Applications*, 2nd ed., Wiley, New York, 2001.
- [29] K. Cho, M.R. Hoffmann, Urea degradation by electrochemically generated reactive chlorine species: products and reaction pathways, *Environ. Sci. Technol.* 48 (2014) 11504–11511.
- [30] C. Cominelli, G.P. Vercesi, Characterization of DSA-type oxygen evolving electrodes – choice of a coating, *J. Appl. Electrochem.* 21 (1991) 335–345.
- [31] H.S. Kong, H.Y. Lu, W.L. Zhang, H.B. Lin, W.M. Huang, Performance characterization of Ti substrate lead dioxide electrode with different solid solution interlayers, *J. Mater. Sci.* 47 (2012) 6709–6715.
- [32] A.G. Scheuermann, J.D. Prange, M. Gunji, C.E.D. Chidsey, P.C. McIntyre, Effects of catalyst material and atomic layer deposited TiO_2 oxide thickness on the water oxidation performance of metal-insulator-silicon anodes, *Energy Environ. Sci.* 6 (2013) 2487–2496.
- [33] E. Tsuji, A. Imanishi, K. Fukui, Y. Nakato, Electrocatalytic activity of amorphous RuO_2 electrode for oxygen evolution in an aqueous solution, *Electrochim. Acta* 56 (2011) 2009–2016.
- [34] S. Marini, P. Salvi, P. Nelli, R. Pesenti, M. Villa, M. Berrettoni, G. Zangari, Y. Kiros, Advanced alkaline water electrolysis, *Electrochim. Acta* 82 (2012) 384–391.
- [35] A. Hug, K.M. Udert, Struvite precipitation from urine with electrochemical magnesium dosage, *Water Res.* 47 (2013) 289–299.
- [36] X. Cheng, Z. Shi, N. Glass, L. Zhang, J.J. Zhang, D.T. Song, Z.S. Liu, H.J. Wang, J. Shen, A review of PEM hydrogen fuel cell contamination: impacts, mechanisms, and mitigation, *J. Power Sources* 165 (2007) 739–756.
- [37] S. Trasatti, Work function, electronegativity, and electrochemical behavior of metals.3. Electrolytic hydrogen evolution in acid solutions, *J. Electroanal. Chem.* 39 (1972) 163.
- [38] M.G. Walter, E.L. Warren, J.R. McKone, S.W. Boettcher, Q.X. Mi, E.A. Santori, N.S. Lewis, Solar water splitting cells, *Chem. Rev.* 110 (2010) 6446–6473.
- [39] E. Navarro-Flores, Z.W. Chong, S. Omanovic, Characterization of Ni, NiMo, NiW and NiFe electroactive coatings as electrocatalysts for hydrogen evolution in an acidic medium, *J. Mol. Catal. A-Chem.* 226 (2005) 179–197.
- [40] C.C.L. McCrory, S. Jung, I.M. Ferrer, S.M. Chatman, J.C. Peters, T.F. Jaramillo, Benchmarking hydrogen evolving reaction and oxygen evolving reaction electrocatalysts for solar water splitting devices, *J. Am. Chem. Soc.* 137 (2015) 4347–4357.
- [41] I.A. Raj, K.I. Vasu, Transition metal-based hydrogen electrodes in alkaline-solution – electrocatalysis on nickel based binary alloy coatings, *J. Appl. Electrochem.* 20 (1990) 32–38.
- [42] R. Solmaz, G. Kardas, Electrochemical deposition and characterization of NiFe coatings as electrocatalytic materials for alkaline water electrolysis, *Electrochim. Acta* 54 (2009) 3726–3734.
- [43] L.D. Munoz, A. Bergel, D. Feron, R. Basseguy, Hydrogen production by electrolysis of a phosphate solution on a stainless steel cathode, *Int. J. Hydrogen Energy* 35 (2010) 8561–8568.
- [44] J.M.C.K. Joe, L.J.J. Janssen, S.J.D. Vanstrelan, J.H.G. Verbunt, W.M. Sluyter, Bubble parameters and efficiency of gas bubble evolution for a chlorine-evolving a hydrogen-evolving and an oxygen-evolving wire electrode, *Electrochim. Acta* 33 (1988) 769–779.
- [45] F.G. Will, Hydrogen plus oxygen recombination and related heat generation in undivided electrolysis cells, *J. Electroanal. Chem.* 426 (1997) 177–184.
- [46] Y. Jiao, Y. Zheng, M.T. Jaroniec, S.Z. Qiao, Design of electrocatalysts for oxygen- and hydrogen-involving energy conversion reactions, *Chem. Soc. Rev.* 44 (2015) 2060–2086.
- [47] J.K. Norskov, J. Rossmeisl, A. Logadottir, L. Lindqvist, J.R. Kitchin, T. Bligaard, H. Jonsson, Origin of the overpotential for oxygen reduction at a fuel-cell cathode, *J. Phys. Chem. B* 108 (2004) 17886–17892.
- [48] H. Vogt, On the gas-evolution efficiency of electrodes. II – numerical analysis, *Electrochim. Acta* 56 (2011) 2404–2410.
- [49] H. Vogt, The rate of gas evolution at electrodes.1. An estimate of the efficiency of gas evolution from the supersaturation of electrolyte adjacent to a gas-evolving electrode, *Electrochim. Acta* 29 (1984) 167–173.
- [50] N. Krstajic, V. Nakic, M. Spasojevic, Hypochlorite production.1. A model of the cathodic reactions, *J. Appl. Electrochem.* 17 (1987) 77–81.

- [51] M. Spasojevic, N. Krstajic, P. Spasojevic, L. Ribic-Zelenovic, Modelling current efficiency in an electrochemical hypochlorite reactor, *Chem. Eng. Res. Des.* 93 (2015) 591–601.
- [52] Y. Tanaka, S. Uchinashi, Y. Saihara, K. Kikuchi, T. Okaya, Z. Ogumi, Dissolution of hydrogen and the ratio of the dissolved hydrogen content to the produced hydrogen in electrolyzed water using SPE water electrolyzer, *Electrochim. Acta* 48 (2003) 4013–4019.
- [53] H. Vogt, The rate of gas evolution at electrodes.2. An estimate of the efficiency of gas evolution on the basis of bubble-growth data, *Electrochim. Acta* 29 (1984) 175–180.
- [54] H. Vogt, On the gas-evolution efficiency of electrodes I – theoretical, *Electrochim. Acta* 56 (2011) 1409–1416.
- [55] S. Shibata, Supersaturation of oxygen in acidic solution in vicinity of an oxygen-evolving platinum anode, *Electrochim. Acta* 23 (1978) 619–623.
- [56] M.H.P. Santana, L.A. De Faria, Oxygen and chlorine evolution on $\text{RuO}_2 + \text{TiO}_2 + \text{CeO}_2 + \text{Nb}_2\text{O}_5$ mixed oxide electrodes, *Electrochim. Acta* 51 (2006) 3578–3585.
- [57] M. Rudolf, I. Rousar, J. Krysa, Cathodic reduction of hypochlorite during reduction of dilute sodium-chloride solution, *J. Appl. Electrochem.* 25 (1995) 155–165.
- [58] C.Y. Cheng, G.H. Kelsall, Models of hypochlorite production in electrochemical reactors with plate and porous anodes, *J. Appl. Electrochem.* 37 (2007) 1203–1217.
- [59] T.J. Schmidt, U.A. Paulus, H.A. Gasteiger, R.J. Behm, The oxygen reduction reaction on a Pt/carbon fuel cell catalyst in the presence of chloride anions, *J. Electroanal. Chem.* 508 (2001) 41–47.
- [60] V.V. Rajasekharan, B.N. Clark, S. Boonsalee, J.A. Switzer, Electrochemistry of free chlorine and monochloramine and its relevance to the presence of Pb in drinking water, *Environ. Sci. Technol.* 41 (2007) 4252–4257.
- [61] S. Verhelst, Recent progress in the use of hydrogen as a fuel for internal combustion engines, *Int. J. Hydrogen Energy* 39 (2014) 1071–1085.
- [62] M.S. Faber, S. Jin, Earth-abundant inorganic electrocatalysts and their nanostructures for energy conversion applications, *Energy Environ. Sci.* 7 (2014) 3519–3542.